Film-Cooling Enhancement In High-Pressure Turbine Of An Aircraft Engine

FILM-COOLING ENHANCEMENT IN HIGH-PRESSURE TURBINE OF AN AIRCRAFT ENGINE

Nabeel Mohammed Al-Zurfi
University of Kufa; University of Manchester
Najaf, Iraq; Manchester, UK
+964 (0) 781 888 3615
nabeelm.alzurfi@uokufa.edu.iq;
nabeel.al-zurfi@manchester.ac.uk

Adel Nasser
University of Manchester
Oxford Road Manchester, UK
+44 (0) 161 306 3537
a.g.nasser@manchester.ac.uk

Ahmed Niameh Alhusseny
University of Kufa; University of Manchester
Najaf, Iraq; Manchester, UK
+964 (0) 7731950978
ahmedn.alhusseini@uokufa.edu.iq;
ahmed.alhusseny@manchester.ac.uk

ABSTRACT

This paper studies the effect of adding vortex generator (VG) at the upstream position of film-holes on a flat-plate simulated turbine blade surface. They are placed at three different positions (0.0m, 0.005m, 0.015m away from film-holes) to investigate the film cooling enhancement. Prism-shaped VG (height: 0.005m, 0.0075m, 0.01m) and prism-shaped VG with inclined top surface (inclined angle: 10°, 20°, 40°) are the configurations that being carried out, at a blowing ratio of M=0.5. The temperature distribution is the main focus is to find out the film-cooling effectiveness by using the commercial StarCCM+ CFD code. The computations of turbulent flow past the stationary blade of gas turbine engines will be modelled using the Reynolds-averaged Navier-Stokes (RANS) equations with sst k-w turbulence model. Several contour diagrams and data plots extracted from the simulation are being used to evaluate the performance of RANS approach for the prediction of the jet-in crossflow (JICF) interaction. The mainstream air and film coolant interaction along the streamwise direction demonstrate how this film-cooling enhancement is worked out effectively. The simulation result shows that mounting the VG at a higher upstream position (further distance away from the film-holes) gives a better film-cooling performance (wider and longer coverage area) and higher film-cooling effectiveness value can be achieved. Top surface inclined prism VG performs generally better than prism VG. VG mounting at a further distance downstream of film-hole is giving a better film-cooling performance.

INTRODUCTION

In film cooling, coolant air is injected through discrete holes drilled at several locations on the blade exterior surface. The performance of the film-cooling is determined by many critical flow and geometric parameters such as the mainstream Reynolds number, blowing ratio, coolant-to-mainstream density ratio, injection angle, rotating speed, turbulence intensity, surface curvature, the shape, size and location of the film hole and so on. Several studies [1-3] have been carried out over the past few decades on the field of a jet in a cross-flow (JICF). Initially, various researches on the cylindrical film-cooling hole have been performed to investigate effects of length and diameter of film holes, blowing ratio, injection angle on film-cooling performance. It was found that the interaction between the coolant jet and mainstream flow results in the formation of highly complex counter-rotating vortex pairs (CRVPs) near the wall surface, and the mixing process is controlled by the dynamics of these vortices. These vortices are detrimental to film cooling and known as the main contributor to the dramatic decrease in the film-cooling effectiveness. Cylindrical film-cooling hole is undoubtedly the simplest and the most economical way of cooling a gas turbine blade but the improvement of the film-cooling performance is limited with blowing ratio beyond the 0.5-1.0 range, which makes it the main disadvantage of the cylindrical holes. Therefore, new film-cooling hole shapes have been studied and designed to satisfy both easy manufacturing and high film-cooling performance. One of those techniques is the anti-vortex concept. It aims to reduce the effect of the CRVPs using a much simpler approach. In the anti-vortex concept, a pair of additional branched coolant jet injection holes branching out from the main cylindrical holes in such a way that the secondary injection destroys the kidney vortices. Besides, the vortex generator (VG) is a flow-control device placed on upstream or downstream of the film cooling holes, to generate streamwise vortices by the protrusion so that CRVP can be controlled, suppressing the effect of CRVP by downwash being induced and reduce the amount of coolant being lifted off. It is proved that it has the ability to improve film cooling performance by acting as a micro-ramp to vary the flow

direction. Neil et al. [4], a change of the surface geometry is developed around the cooling hole. The VG design could produce ACRVPs downstream as well to achieve a better cooling performance. Vortex generator can also be mounted beyond the film-cooling hole which is the downstream position. Khorsi et al. [5] has predicted the improvement of film-cooling performance by placing a crescent-shaped (moon-shaped) block as a flow controlling device at the downstream of a cylindrical hole at different blowing ratios. It was clear that the film-cooling effectiveness in the intermediate region of the hole with the device is significantly higher than that in the case without the device. The presence of downstream vortex generator spreads the coolant from the cylindrical hole in lateral direction while it was passing over the top of the device. David et al. [6] has demonstrated to set up a single delta vortex generator placed downstream of a 30-degree angled cylindrical film-cooling hole. It was noticed that the flow near the plate was pulled between the vortices while coolant between vortex pair was forced up away from the wall. With an increase in blowing ratio, the vortex was pushed further away from the plate causing a little interaction between coolant and the plate surface. Zaman et al.[7] and Aaron et al. [8] have done studies also with a delta vortex generator. It was found that there was a low temperature region at the leading-edge of the jet which was caused by a horseshoe vortex that entrained coolant and redistributed it along the wall. The location of the vortex generator (VG) can cause a big influence on the film-cooling performance. For placing an upstream VG, the film-cooling performance improves with an increasing upstream distance. The film-cooling performance improves first then impairs with increasing VG gaps. When considering upstream distance on film-cooling performance, the influence of twisted flow which is opposite rotation of CRVP decrease with an increase in upstream distance away from the VG. The increase of VG distance causes the coolant to be less uniform in spanwise direction, leading to an attenuated film. For placing an uptream vortex generator, the study of Zaman et al. [9] shows that the effect of heights and locations both have an effect on film-cooling performance. The increase in height of VG causes the jet core to dissipate gradually because of the larger turbulence intensity. Placing it over a distance of three diameters from the film-cooling hole would show the least lift-off impact. Moreover, according to studies from Daren et al. [10], when the influence of gap between a double VG is considered, the intensity of twisted flow which is in opposite rotation of CRVP goes up then goes down with an increase gap distance. Reducing the distance between VGs increase the intensity of the vortices but the gap must be optimal in order to ensure recovery of the surface of the wall while avoiding the coalescence of vortices with a smaller distance. In terms of the shape of vortex generator (VR), according to Zheng et al. [11], comparison between rectangular shape, triangular shape, parallelogram shape, and trapezoid shape double VG have been made. The result shows that parallelogram-shaped VG has the highest total pressure loss coefficient. In the bottom corner of a parallelogram-shaped VG, a few vorticity pairs were observed which increased the total pressure loss. However, they performed the best film-cooling performance among different shapes despite their high-pressure loss penalty. To compensate between film-cooling effectiveness and press loss, triangular-shaped VG would be a choice to obtain a balance.

NOMENCLATURE

M	[-]	*Blowing ratio*
P	[N.m^{-2}]	Pressure
T	[K]	Local temperature
ρ	[kg /m^3]	Fluid density
μ	[N·s/m^2]	Dynamic viscosity
μ_t	[N·s/m^2]	Turbulent viscosity
VG	[-]	Vortex generator
x	[m]	Cartesian axis direction
y	[m]	Cartesian axis direction
z	[m]	Cartesian axis direction
Special characters		
η	[-]	Film cooling effectiveness
Subscripts		
C		Coolant
∞		Free stream

MATHEMATICAL FORMULATION

In the present study, the fluid is assumed as Newtonian fluid, and the flow is considered to be turbulent, steady, incompressible, and three-dimensional. Based on these assumptions, the governing and transport equations are [12]:

$$\frac{\partial}{\partial x_i}(\rho u_i) = 0 \tag{1}$$

$$\frac{\partial}{\partial x_j}(\rho u_i u_j) = -\frac{\partial p}{\partial x_i} + \frac{\partial}{\partial x_j}\left[(\mu + \mu_t)\left(\frac{\partial u_i}{\partial x_j} + \frac{\partial u_j}{\partial x_i}\right)\right] - \frac{2}{3}\frac{\partial}{\partial x_j}\rho k\delta_{ij} + S_{\emptyset i} \tag{2}$$

$$\frac{\partial}{\partial x_i}(\rho T u_i) = \frac{\partial}{\partial x_i}\left[\left(\frac{\mu}{Pr} + \frac{\mu_t}{Pr_t}\right)\frac{\partial T}{\partial x_i}\right] \tag{3}$$

To find the turbulent eddy viscosity (μ_t), the Menter k–ω SST turbulence model was employed in the present study as follows [12]:

$$\frac{\partial}{\partial x_i}(\rho k u_i) = \frac{\partial}{\partial x_i}\left[\left(\mu + \frac{\mu_t}{\sigma_k}\right)\frac{\partial k}{\partial x_i}\right] + 2\mu_t\delta_{ij}.\delta_{ij} - \frac{2}{3}\rho k\frac{\partial u_i}{\partial x_j}\delta_{ij} - \beta_1\rho k\omega \tag{4}$$

$$\frac{\partial}{\partial x_i}(\rho\omega u_i) = \frac{\partial}{\partial x_i}\left[\left(\mu + \frac{\mu_t}{\sigma_{\omega 1}}\right)\frac{\partial \omega}{\partial x_i}\right] + \gamma\left(2\rho\delta_{ij}.\delta_{ij} - \frac{2}{3}\rho\omega\frac{\partial u_i}{\partial x_j}\delta_{ij}\right) - \beta_2\rho\omega^2 + 2\frac{\rho}{\sigma_{\omega 2}\omega}\frac{\partial k}{\partial x_k}\frac{\partial \omega}{\partial x_k} \tag{5}$$

where $S_{\phi i}$ is the source term of the momentum equation, $P_k = 2\mu_t \delta_{ij}.\delta_{ij} - \frac{2}{3}\rho k \frac{\partial u_i}{\partial x_j}\delta_{ij}$ is the rate of production of turbulent kinetic energy, and $\delta_{ij} = \frac{1}{2}\left(\frac{\partial u_i}{\partial x_j} + \frac{\partial u_j}{\partial x_i}\right)$.

The turbulent eddy viscosity is defined as: $\mu_t = \rho k/\omega$

The values of the empirical constants and turbulent Prandtl number in equations 1-5 are defined as:
$\sigma_k = 1.0,\ \sigma_{\omega 1} = 2.0,\ \sigma_{\omega 2} = 1.17,\ \gamma = 0.44,\ \beta_1 = 0.09,\ \beta_2 = 0.083,\ Pr_t = 0.9$

PHYSICAL MODEL

This simulation is validated based on Chao et al. [13] experimental setup. It is a flat plate modelling simulation that represent a turbine blade in an aircraft engine. The 3D-CAD model is drawn by StarCCM+ code. There are a total of 3 bodies; the mainstream cuboid with two revolved cut vortex generator and inlet coolant pipes x2. The mainstream flow is demonstrated by a cuboid as shown in figure 1. It has a dimension of 0.06 m (W) x 0.03 m (H) x 0.25 m (L). Two cylindrical pipes are extruded from the middle bottom to demonstrate coolant injection. They have a diameter (D) of 0.005m and extruded at a length of 0.1m. The pipes and the cuboid formed an inclined angle of 30 degrees. The pipes are connected with the cuboid by creating an interface at the intersection circle. This allows the coolant to be injected into the mainstream. The global origin (0,0,0) is set at the centre of the cuboid. Mainstream flow at positive X-direction while coolant is joining them from the film-holes.

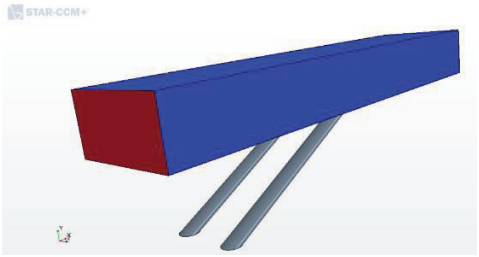

Figure 1 Cuboid section (mainstream)

A vortex generator pair is mounted at the upstream location before the film-cooling hole. It is a triangular prism shaped extrusion cut. And a triangular prism with an inclined top surface revolved cut is also compared with a same height prism to see the effect. Vortex generators is known to be able to generate anti-vortex (ACRVP) which favour film-cooling effectiveness. A twisted flow rotates in the opposite direction of kidney vortices can attenuate its effects

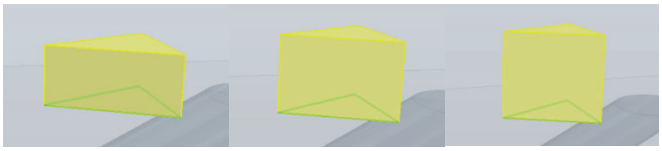

Figure 2 Prism-shaped VG: (a) 0.005m, (b) 0.0075m, (c) 0.01m

In most cases, modification on the location, shape of film-hole is being focused while shaped of VG is rarely considered.

This research is further exploring the effect by changing the shaped of VG itself. A total of 6 different shapes of VG are tested in three locations. Figure 2 is prism-shaped VG with height of 0.005m (D), 0.0075m (1.5D), 0.01m (2D). Figure 3 is top-surface inclined VG with inclined-angle of 10°, 20°, 40°.

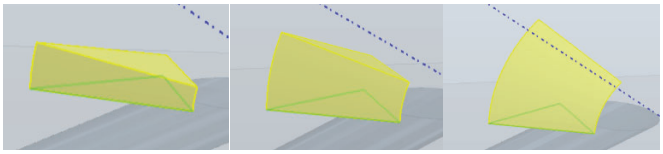

Figure 3 Inclined VG: (a) 10°, (b) 20°, (c) 40°

These VGs are placed at the up-stream location before each film hole. Three different locations are being tested: 0.0 m, 0.005m, 0.015m away from the hole. They are presented in figure 4 below.

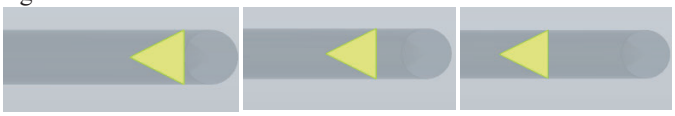

Figure 4 VG positions

Boundary treatments and flow conditions

The mainstream inlet velocity (u_∞) and inlet total temperature (T_∞) are 23 m/s and 293 K, respectively. A turbulence intensity of 2.7% and a turbulence length scale of 3% of the flat plate length are applied at the mainstream inlet. The flow outlet condition of the flat plate is set as a pressure-outlet with the static pressure P_{out}=101325 Pa. The periodic boundary condition is imposed in the symmetry planes. Relatively cooler air is employed as a coolant to protect the plat surface from the hot mainstream. The coolant air is directly introduced into the film hole inlet sections by adopting a velocity inlet. The total temperature of the coolant flow (T_c) is taken to be 263 K, so that the coolant-to-mainstream density ratio (DR) is about 1.7, as in an engine, and the inlet velocity is determined according to the blowing ratio. The inlet of each film hole is defined as a velocity inlet, and the outlet is defined as an in-place interface between the plat surface and the film hole exit. An adiabatic no-slip condition is applied for the solid wall boundaries of the flat plate and film holes.

Furthermore, the simulations were performed for different inlet temperatures of the coolant and mainstream, which significantly affect the hydrodynamic behaviours of the proposed problem. This temperature difference causes variations in flow properties, especially near the hole exit. Thus, Sutherland's laws for viscosity and thermal conductivity and the ideal gas law for an incompressible flow were used to express the dynamic viscosity, thermal conductivity, and fluid density, respectively, as a function of the flow temperature in order to compute the spatial variation of flow properties throughout the computational domain except the boundary values.

GRID SYSTEM

Two multi-block grids were generated using starccm+ software, one covering the flat plate and a second one inside the film holes. The domain of the flat plat was composed entirely of polyhedral meshes with prism layer meshes, which are more accurate with less numerical diffusion. Detailed grid distribution is shown in figure 5. The prism layer is set so that the mesh is finer near the wall on the flat plate. The mesh was stretched away

from the viscous wall using a stretching ratio of 1.205. A first height of 0.0172 mm was used in order to accurately capture the boundary layer region. The second domain, on the other hand, consisted of two rows of film holes. These two block meshes were then merged together to form a "hybrid" mesh, with a non-conformal interface boundary between them. For computational accuracy, the ratio of two adjacent grid sizes in any direction was kept within 0.87-1.15. No wall functions were used; thus viscous clustering was employed at all solid walls with a Y+ value of less than 1.0 for the first grid point off the wall at all locations. The total grid number was approximately 3,000,000 for all bodies.

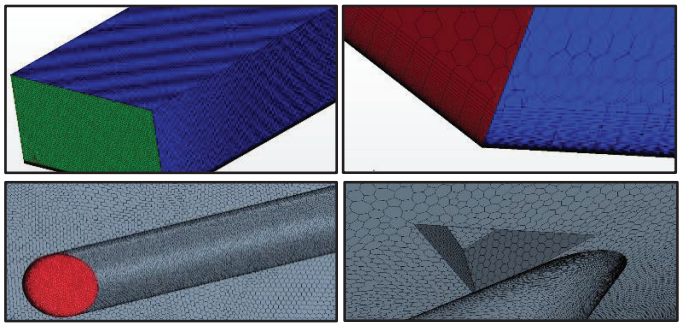

Figure 5 Grid structures for the VG design

Validation

The lateral-averaged film-cooling effectiveness experimental result from Chao et al. [13] is used to validate the results of the model from StarCCM+.The curve of M=0.5 is chosen for validating the result as shown in figure 6.

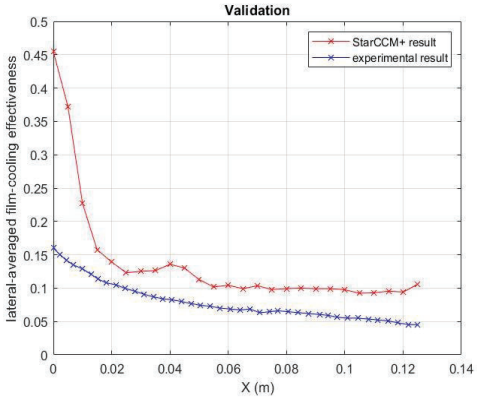

Figure 6 StarCCM+ and experimental result plots of blowing ratio= 0.5

The difference between results is very small. The change of lateral-averaged film-cooling effectiveness along the streamwise direction is the same at both studies. As the model is done by RANS which has a less accuracy, the slight difference of exact film-cooling effectiveness value is acceptable.

Results and discussion

The cooling performance of 6 configurations at 3 locations are systematically showing the effect of VG at cylindrical hole at M=0.5. Adding a VG in upstream position of each film-hole is investigated in this paper as a way to increase film-cooling effectiveness. VG is mounted in 3 locations with 3 different heights. A clear improvement is visible in the contour diagrams. Moreover, the VG is then modified by having an inclined top-surface with 3 different degree of angles towards the film hole at 3 locations. The first part of this section shows the contour diagram in different views showing the flow mechanism of temperature distributions. The second part is extracting data from the contour diagram and presenting in plotted graph to show the global lateral film-cooling effectiveness distribution.

1-Temperature contour diagrams (prism VG) with blowing ratio of 0.5

As shown in figure 7, the film-cooling effectiveness of VG at blowing ratio of 0.5 with height of 0.005m, 0.0075m, 0.01m are placed at three distances 0.0m, 0.005m, 0.015m away from the film-holes. It is worth noted that the VG and film-holes location are not taken into account, as the contour diagram is considering the protection on the flat plate surface itself.

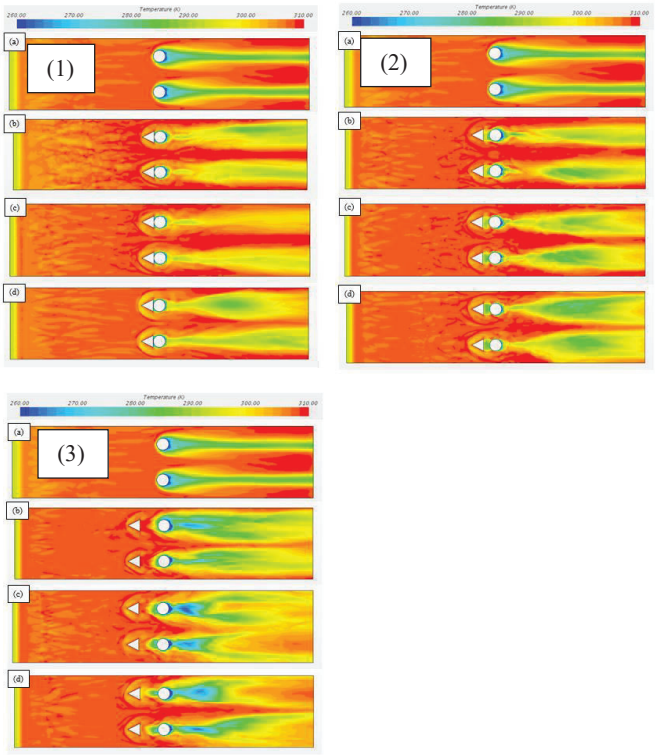

Figure 7 Temperature contour diagram with a distance of (1) 0.0m, (2) 0.005, and (3) 0.015 away from film-holes at different height of VG: (a) no VG, (b) 0.005m, (c) 0.0075m, and (d) 0.01m.

From figure 7-1, adding a VG can clearly show a larger coverage area of film cooling, the lift-off phenomenon is suppressed as in Fig. 7-1b, 7-1c, and 7-1d. Adjusting the height of VG also plays a role on affecting the coverage area, 0.005m in Fig. 7-1b and 0.01m in Fig. 7-1d shows a better coverage than 0.0075m in Fig. 7-1c. With a higher height of VG is seen to be having the largest coverage area throughout the surface. It has a distinct film coverage in the area just beyond the film-hole while the other two shorter height give a blur result.

Then, the VGs are moved away from the film-holes at a position 0.005m away. In figure 7-2, it is clear that a taller VG

gives a larger coverage area along streamwise direction. Comparing the area just beyond the film-holes, in Fig. 7-2b, 0.005m height shows the weakest film-cooling protection while increasing the height gives better performance in those areas. However, comparing Fig. 7-1 and 7-2, the overall performance in the beyond hole area is better for a closer VG.

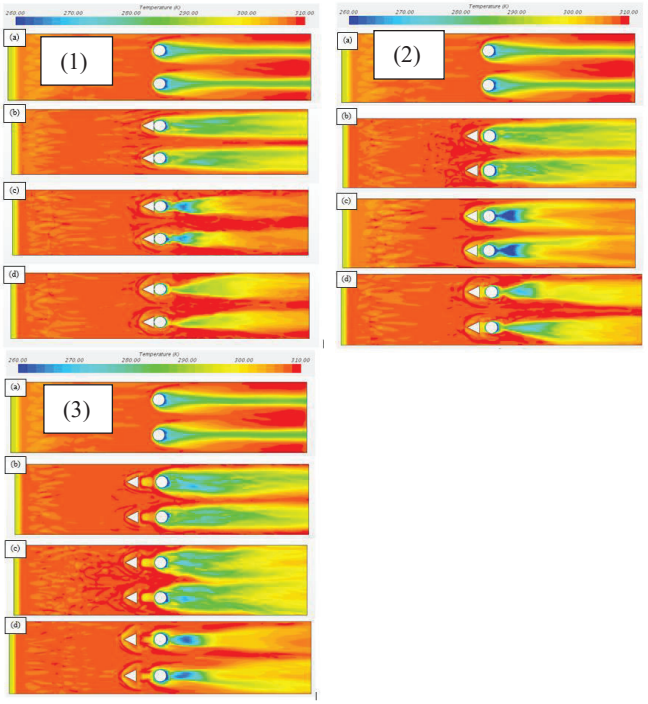

Figure 8 Temperature contour diagram with a distance of (1) 0.0m, (2) 0.005, and (3) 0.015 away from film-holes at different inclined-top-surface of VG: (a) no VG, (b) 10°, (c) 20°, and (d) 40°.

In figure 7-3, moving the VG to a further distance of 0.015m away from film-holes, the film-cooling effectiveness becomes very significant with areas reaching η>0.8. In Fig. 7-3b, a 0.005m height VG can give a larger area of film protection along the streamwise compare to 0.0075m and 0.01m in Fig. 7-3c and Fig. 7-3d. While for 0.0075m and 0.01m height of VG, they have a higher film-cooling effectiveness in the area beyond the film-holes. In Fig 7-3c, 0.0075m VG is the only case that can combine two separate film-cooling flow together. However, the shortest 0.005m gives the best evenly distributed film-cooling performance while the other higher two give a swallowtail shape in further downstream area.

In figure 8, VGs with their top surface being inclined towards the film-hole at 10°, 20°, and 40° with blowing ratio of 0.5 are placed at three distances 0.0m, 0.005m, 0.0015m away from the film-holes.

In figure 8-1, a VG with top surface inclined towards the film-hole with different degrees are demonstrated at a distance of 0.0m away from the film-hole. Compare 10°, 20°, and 40° of inclination in Fig. 8-1b, c, d, 10° gives the largest area of coverage streamwise and spanwise while 20° and 40° both give a funnel-shaped coverage at the area just beyond the film-hole. 20° VG gives a higher value of film-cooling effectiveness at the area beyond the film-hole while 40° VG perform a longer and further coverage than 20° VG.

2-Lateral film cooling effectiveness (prism VG) with blowing ratio of 0.5.

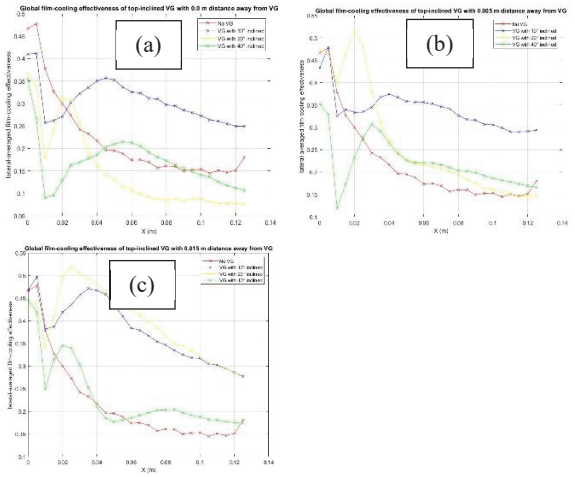

Figure 1 Global film-cooling effectiveness distribution of prism VG with distance (a) 0.0m, (b) 0.005m, (c) 0.015m.

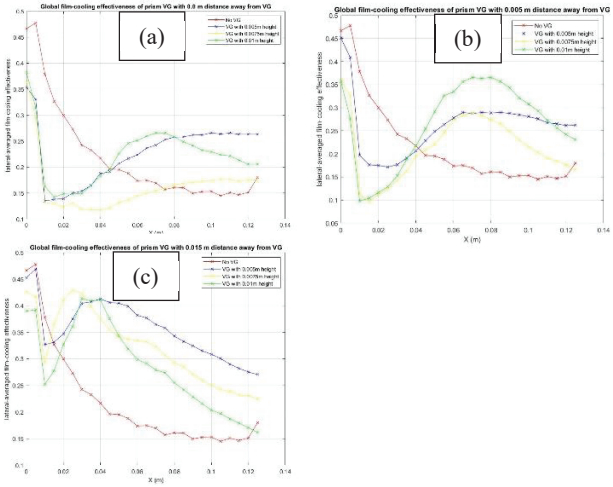

Figure 10 Global film-cooling effectiveness distribution of prism VG with top inclined surface with distance (a) 0.0m, (b) 0.005m, (c) 0.015m.

In figure 8-2, the VGs are moved to a distance of 0.005m away from film-hole. The film-cooling effectiveness becomes much more distinct. In Fig. 8-2b, the 10° VG still gives the largest overall area of film coverage. 10° and 20° VG in Fig. 8-2c & d give a funnel-shaped film coverage just beyond the film-hole. 20° VG has the highest value of film effectiveness among all but the coverage ends shorter than 40°. It is worth knowing that although 20° VG gives a funnel shape, it is actually surrounded by an area of film coverage but with a smaller effectiveness value. In figure 8-3, the VG is mounted at 0.015m away from the film-hole. It is very clear that Fig. 8-3c, the 20° VG gives the best area of coverage with both coverage of two

separate films now merged together. 10° VG in fig. 8-3b, also gives a large area of coverage but it is less even than the 20° VG. In Fig. 8-3d, it has the highest effectiveness at the area beyond film-hole but the overall film-coverage is very narrow and small compare with the other two.

Figures 9 and 10 show the lateral-averaged film-cooling effectiveness distributions of both VG configurations (0.0m, 0.005m, 0.015m) and (10°, 20°, 40°) at blowing ratio of 0.5. These distributions are much more useful than the local values as they are extracted from 26 spanwise line probes which the averaged values of each line probe are then used to plot these graphs. Therefore, the plots have a more stable values and less fluctuated. Moreover, these distributions are able to tell the film coverage spanwisely by averaging the values which are more significant for investigations of VG effect. In figure 9a, the global values of prism VG at 0.0m distance shows that the adding of VGs cause a sharp decline but then the effectiveness will rise back after reaching a trough. Lastly, cases with VG perform better than without VG. The order is as follow: 0.005m VG>0.01m VG>0.0075m VG>no VG. In figure 9b, distance of 0.005m, the trends of curves are the same as 0.0m. The 0.005m VG has a less decline compare to other two heights and it does not have a second decline the other two does from X(m)=0.07. The order is as follow: 0.01m VG>0.005m VG>0.0075m VG>no VG. Lastly, the distance 0.01m in figure 9c, the three curves perform similarly. All the VGs case perform better than without a VG. The order is: 0.005m VG>0.0075m VG>0.01m VG>no VG. In figure 10a, with a distance of 0.0m, the inclined VGs only have 10° inclined VG performs better than no VG. 20° inclined VG performs badly that it has a sudden raise at X(m)=0.02 for a value of 0.3 while 40° inclined VG has a decline at first but then back to same level as no VG. In figure 10b, at distance 0.005m, 20° inclined VG has the least decline follows by 10° then 40°. 20° inclined VG rises to the highest peak among all follows by 10° then 40°. However, only 10° inclined VG can maintain the effectiveness along streamwise direction, leaving 20° and 40° inclined VG drops to a level that is slightly higher than no VG case. In figure 10c, at distance of 0.015m, all the VGs trend has perform similarly. They first drop, then reach a peak, and lastly decline again. At this distance, 10° and 20° inclined VG have higher value of film-cooling effectiveness. 40° inclined VG has a very low value similar to no VG curve. The order is as follow: 20°>10°>40°>no VG.

Conclusion

In this study, the shapes of VG are newly designed to measure the effectiveness at a blowing ratio of M=0.5. The main conclusions are drawn as follows:

1-The distance of 0.015m between VG and film-hole gives the best film-cooling performance among all configurations.

2-For prism VG, 0.005m height and 0.0075m height gives the largest film-coverage at M=0.5.

3-For top surface inclined prism VG, 20° inclined VG gives the largest film-coverage at M=0.5.

4-ACRVP is the key to suppress CRVP, the strongest ACRVP can be found in 0.0075m height prism VG and 0.01 height prism VG at distance of 0.015m at M=0.5. Overall, a taller VG is able to produce a bigger ACRVP. For inclined VG, 20° inclined VG produces the strongest ACRVP that is able to suppress CRVP but also flattening themselves to give a large coverage at M=0.5.

5-At a blowing ratio of M=0.5, 0.005m VG, 10° inclined VG, and 20° inclined VG at 0.015m distance give the highest lateral-averaged film-cooling effectiveness value which is nearly 200% improvement.

6-A top surface inclined prism VG gives a better film-cooling performance than normal prism VG in terms of film-coverage area and lateral-averaged film-cooling effectiveness but the inclination angle cannot be too extreme. An angle of around 20° is an ideal configuration.

REFERENCES

[1] Ito, S., Goldstein, R.J. and Eckert, E.R.G. 1978. Film Cooling of a Gas Turbine Blade. *Journal of Engineering for Power*. 100, 3 (1978), 476. DOI:https://doi.org/10.1115/1.3446382.

[2] Andreopoulos, J. and Rodi, W. 1984. Experimental investigation of jets in a crossflow. *Journal of Fluid Mechanics*. 138, 1 (Jan. 1984), 93. DOI:https://doi.org/10.1017/S0022112084000057.

[3] Kelso, R.M., Lim, T.T. and Perry, A.E. 1996. An experimental study of round jets in cross-flow. *Journal of Fluid Mechanics*. 306, 1 (Jan. 1996), 111. DOI:https://doi.org/10.1017/S0022112096001255.

[4] Neil Titchener, Holger Babinsky, 2015. A review of the use of vortex generators for mitigating shock-induced separation. Shock Waves, pp. 473-494.

[5] A. Khorsi, A. Guelailia, and M. K. Hamidou, 2016. Improvement of film cooling effectiveness with a small downstream block body. Journal of applied mechanics and technical physics, 57(4), pp. 666-671.

[6] David L. Rigby, James D. Heidmann, 2008. Improved film cooling effectiveness by placing a vortex generator downstream of each hole. power for land, sea and air.

[7] Zaman, K. B. M. Q., Rigby, D. L., Heidmann, J. D., 2010. Experimental Study of an Inclined Jet-In-Cross-Flow Interacting With a Vortex Generator, 48th AIAA Aerospace Sciences Meeting Including the New Horizons Forum and Aerospace Exposition 4 - 7 January 2010, Orlando, Florida

[8] Aaron F. Shinn, S. Pratap Vanka, 2013. Large Eddy Simulations of Film-Cooling Flows With a Micro-Ramp Vortex Generator. Journal of Turbomachinery, Volume 135.

[9] Zaman K, Rigby DL, Heidmann JD, 2010. Inclined jet in crossflow interacting with a vortex generator. J Propul Power 26 (5); 947-954.

[10] Daren Zheng, Xinjun Wang, Qi Yuan, 2019. Numerical Investigation on the Effects of Vortex Generator Locations on Film Cooling Performance. Int J Turbo Jet Eng, Vol.1, Issue 1, https://doi.org/10.1515/tjj-2019-0024

[11] D. Zheng, X. Wang, Q. Yuan, 2019. Numerical investigation on the effect of vortex generator shapes on film cooling performance. Thermophysics and Aeromechanics, 26, pp. 445-460.

[12] H K Versteeg and W Malalasekera, An Introduction to Computational Fluid Dynamics, Second Edi. England: Pearson education, 2007.

[13] Chao Zhang, Jie Wang, Xurbin Liu, Liming Song, Jun Li, Zhenping Feng, 2020. Experimental and Numerical Study on the Flat-Plate Film Cooling Enhancement Using the Vortex Generator Downstream for the Fan-Shaped Hole Configuration. Journal of Turbomachinery, 142(3): 031006 (13 pages), Paper No: TURBO-19-1293 https://doi.org/10.1115/1.4046234.